Belle Preprint 2007-46
KEK Preprint 2007-55
arXiv: 0711.3252

Study of $B \to D^{**}\ell\nu$ with full reconstruction tagging

D. Liventsev,[11] I. Adachi,[7] H. Aihara,[39] K. Arinstein,[1] T. Aushev,[16,11] A. M. Bakich,[36] V. Balagura,[11] E. Barberio,[19] A. Bay,[16] U. Bitenc,[12] A. Bondar,[1] A. Bozek,[25] M. Bračko,[18,12] J. Brodzicka,[7] T. E. Browder,[6] P. Chang,[24] Y. Chao,[24] A. Chen,[22] K.-F. Chen,[24] W. T. Chen,[22] B. G. Cheon,[5] R. Chistov,[11] I.-S. Cho,[44] Y. Choi,[35] S. Cole,[36] J. Dalseno,[19] M. Danilov,[11] M. Dash,[43] A. Drutskoy,[3] S. Eidelman,[1] D. Epifanov,[1] N. Gabyshev,[1] B. Golob,[17,12] H. Ha,[14] J. Haba,[7] K. Hayasaka,[20] H. Hayashii,[21] M. Hazumi,[7] D. Heffernan,[30] Y. Hoshi,[38] W.-S. Hou,[24] Y. B. Hsiung,[24] H. J. Hyun,[15] T. Iijima,[20] K. Inami,[20] A. Ishikawa,[32] H. Ishino,[40] R. Itoh,[7] M. Iwasaki,[39] Y. Iwasaki,[7] D. H. Kah,[15] J. H. Kang,[44] P. Kapusta,[25] H. Kawai,[2] T. Kawasaki,[27] H. Kichimi,[7] H. J. Kim,[15] Y. J. Kim,[4] K. Kinoshita,[3] S. Korpar,[18,12] P. Križan,[17,12] P. Krokovny,[7] R. Kumar,[31] C. C. Kuo,[22] A. Kuzmin,[1] Y.-J. Kwon,[44] J. S. Lee,[35] M. J. Lee,[34] S. E. Lee,[34] T. Lesiak,[25] A. Limosani,[19] S.-W. Lin,[24] Y. Liu,[4] F. Mandl,[9] S. McOnie,[36] T. Medvedeva,[11] H. Miyake,[30] H. Miyata,[27] Y. Miyazaki,[20] R. Mizuk,[11] D. Mohapatra,[43] G. R. Moloney,[19] E. Nakano,[29] M. Nakao,[7] H. Nakazawa,[22] Z. Natkaniec,[25] S. Nishida,[7] O. Nitoh,[42] T. Nozaki,[7] S. Ogawa,[37] T. Ohshima,[20] S. Okuno,[13] S. L. Olsen,[6,8] H. Ozaki,[7] P. Pakhlov,[11] G. Pakhlova,[11] C. W. Park,[35] H. Park,[15] K. S. Park,[35] R. Pestotnik,[12] L. E. Piilonen,[43] Y. Sakai,[7] O. Schneider,[16] C. Schwanda,[9] K. Senyo,[20] M. Shapkin,[10] H. Shibuya,[37] J.-G. Shiu,[24] B. Shwartz,[1] A. Sokolov,[10] A. Somov,[3] S. Stanič,[28] M. Starič,[12] T. Sumiyoshi,[41] S. Suzuki,[32] F. Takasaki,[7] M. Tanaka,[7] G. N. Taylor,[19] Y. Teramoto,[29] I. Tikhomirov,[11] S. Uehara,[7] K. Ueno,[24] T. Uglov,[11] Y. Unno,[5] S. Uno,[7] P. Urquijo,[19] Y. Usov,[1] G. Varner,[6] K. Vervink,[16] S. Villa,[16] A. Vinokurova,[1] C. C. Wang,[24] C. H. Wang,[23] M.-Z. Wang,[24] P. Wang,[8] X. L. Wang,[8] Y. Watanabe,[13] E. Won,[14] Y. Yamashita,[26] Z. P. Zhang,[33] V. Zhilich,[1] A. Zupanc,[12] and O. Zyukova[1]

(The Belle Collaboration)

[1]*Budker Institute of Nuclear Physics, Novosibirsk*
[2]*Chiba University, Chiba*
[3]*University of Cincinnati, Cincinnati, Ohio 45221*
[4]*The Graduate University for Advanced Studies, Hayama*
[5]*Hanyang University, Seoul*
[6]*University of Hawaii, Honolulu, Hawaii 96822*
[7]*High Energy Accelerator Research Organization (KEK), Tsukuba*
[8]*Institute of High Energy Physics, Chinese Academy of Sciences, Beijing*
[9]*Institute of High Energy Physics, Vienna*
[10]*Institute of High Energy Physics, Protvino*
[11]*Institute for Theoretical and Experimental Physics, Moscow*
[12]*J. Stefan Institute, Ljubljana*
[13]*Kanagawa University, Yokohama*
[14]*Korea University, Seoul*
[15]*Kyungpook National University, Taegu*
[16]*École Polytechnique Fédérale de Lausanne (EPFL), Lausanne*
[17]*Faculty of Mathematics and Physics, University of Ljubljana, Ljubljana*

[18] University of Maribor, Maribor
[19] University of Melbourne, School of Physics, Victoria 3010
[20] Nagoya University, Nagoya
[21] Nara Women's University, Nara
[22] National Central University, Chung-li
[23] National United University, Miao Li
[24] Department of Physics, National Taiwan University, Taipei
[25] H. Niewodniczanski Institute of Nuclear Physics, Krakow
[26] Nippon Dental University, Niigata
[27] Niigata University, Niigata
[28] University of Nova Gorica, Nova Gorica
[29] Osaka City University, Osaka
[30] Osaka University, Osaka
[31] Panjab University, Chandigarh
[32] Saga University, Saga
[33] University of Science and Technology of China, Hefei
[34] Seoul National University, Seoul
[35] Sungkyunkwan University, Suwon
[36] University of Sydney, Sydney, New South Wales
[37] Toho University, Funabashi
[38] Tohoku Gakuin University, Tagajo
[39] Department of Physics, University of Tokyo, Tokyo
[40] Tokyo Institute of Technology, Tokyo
[41] Tokyo Metropolitan University, Tokyo
[42] Tokyo University of Agriculture and Technology, Tokyo
[43] Virginia Polytechnic Institute and State University, Blacksburg, Virginia 24061
[44] Yonsei University, Seoul

Abstract

We report a study of semileptonic B decays to P-wave D^{**} mesons. Semileptonic decay to a D_2^* meson is observed for the first time and its product branching ratio is measured to be $\mathcal{B}(B^+ \to \bar{D}_2^{*0}\ell^+\nu) \times \mathcal{B}(\bar{D}_2^{*0} \to D^-\pi^+) = 0.22 \pm 0.03(\text{stat.}) \pm 0.04(\text{syst.})\%$. The result is obtained using fully reconstructed B tags from a data sample that contains $657 \times 10^6 B\bar{B}$ pairs collected at the $\Upsilon(4S)$ resonance with the Belle detector at the KEKB asymmetric-energy e^+e^- collider.

PACS numbers: 13.20.-v, 13.20.He, 14.40.Lb

Heavy Quark Effective Theory (HQET) has proven to be very successful at describing semileptonic decays of B-mesons, especially inclusive transitions; it allows one to extract $|V_{cb}|$ to better than 2% accuracy [1]. However, some difficulties arise when it is applied to exclusive decays. For example, certain sum rules (in particular, the Uraltsev sum rule [2]) imply the strong dominance of decays to the narrow excited D mesons over those to the wide excited D mesons, while some experimental data show the opposite trend [3, 4]. However, no complete experimental study of such semileptonic decays to excited D-mesons exists, and thus no direct comparison with theoretical predictions can be performed. In this paper we report on a study of $B \to D^{(*)}\pi\ell\nu$ decays and measure the excited D contributions to the $D^{(*)}\pi$ final state.

According to HQET there are two doublets of orbitally excited (P-wave) charmed mesons (D^{**}), differentiated by their light quark angular momentum $j_q = 1/2$ or $j_q = 3/2$. Members of the $j_q = 3/2$ doublet are predicted to decay only via a D-wave and be relatively narrow, while members of the $j_q = 1/2$ doublet are predicted to decay only via an S-wave and be relatively broad [5]. The D^{**} states with spin-parity and light quark angular momentum combinations $0^+(j_q = 1/2)$, $1^+(j_q = 1/2)$, $1^+(j_q = 3/2)$ and $2^+(j_q = 3/2)$ are usually labelled D_0^*, D_1', D_1 and D_2^*, respectively. The D^{**} states have previously been observed and studied in hadronic B-decays [6]. Semileptonic B decays to narrow D_1 and D_2^* mesons have been studied by a number of experiments [7]. The semileptonic branching fractions of $B \to D^{(*)}\pi\ell\nu$ decays were recently measured by Belle [8] and BaBar [9].

This measurement is based on a data sample that contains 657 million $B\bar{B}$ pairs, which corresponds to $605\,\mathrm{fb}^{-1}$, collected at the $\Upsilon(4S)$ resonance with the Belle detector operating at the KEKB asymmetric-energy e^+e^- collider [10]. An additional $68\,\mathrm{fb}^{-1}$ data sample taken at a center-of-mass energy 60 MeV below the $\Upsilon(4S)$ resonance is used to study continuum $e^+e^- \to q\bar{q}$ ($q = u, d, s, c$) background. The Belle detector is a large-solid-angle magnetic spectrometer that consists of a silicon vertex detector (SVD), a 50-layer central drift chamber (CDC), an array of aerogel threshold Cherenkov counters (ACC), a barrel-like arrangement of time-of-flight scintillation counters (TOF), and an electromagnetic calorimeter comprised of CsI(Tl) crystals (ECL) located inside a superconducting solenoid coil that provides a 1.5 T magnetic field. An iron flux-return located outside the coil is instrumented to detect K_L^0 mesons and to identify muons (KLM). The detector is described in detail elsewhere [11]. Two inner detector configurations were used. A 2.0 cm beam pipe and a 3-layer silicon vertex detector was used for the first sample of 152 million $B\bar{B}$ pairs, while a 1.5 cm beam pipe, a 4-layer silicon detector and a small-cell inner drift chamber were used to record the remaining 504 million $B\bar{B}$ pairs [12].

To suppress the large combinatorial background expected in the reconstruction of final states including a neutrino, we use a full reconstruction tagging method, which has been improved in comparison with our previous paper [8]. The first B meson (denoted as $B_{\rm sl}$) is reconstructed in the semileptonic mode of interest, *i.e.* as a combination of all final particles $D^{(*)}\pi\ell$ except for the neutrino. The remainder of the event is combined into either a $D^{(*)}\mathrm{n}\,\pi^{\pm}$ ($\mathrm{n} \leq 6$) or $D^{(*)}\rho^-$ combination to form the tagging B meson (referred to below as $B_{\rm tag}$). Semileptonic decays are identified by a peak around zero in the missing mass squared spectrum, $M_\nu^2 = (P_{\rm beams} - P_{\rm tag} - P_{\rm sl})^2$, where $P_{\rm beams}$ is the total four-momentum of the beams and $P_{\rm tag}$ and $P_{\rm sl}$ are the reconstructed four-momenta of the $B_{\rm sl}$ and $B_{\rm tag}$, respectively. This method provides significantly improved resolution in the missing momentum in comparison with non-tagging methods, thus allowing background suppression, separation of different decay modes and precise calculation of the decay kinematics.

Charged tracks are required to originate from the interaction point (IP). Charged tracks positively identified as electrons or muons with $|\vec{P}| > 1.0\,\mathrm{GeV}/c$ are used as leptons. Charged kaons are identified by combining information on track ionization loss (dE/dx), Cherenkov light yields and time-of-flight information. No pion identification is required. Photons are identified as isolated electromagnetic showers with energies greater than 50 MeV that are not matched to any charged track.

K^0_S mesons are reconstructed from $\pi^+\pi^-$ pairs having an invariant mass within $\pm 30\,\mathrm{MeV}/c^2$ ($\pm 5\sigma$) of the nominal K^0_S mass and a well reconstructed vertex displaced from the IP. π^0 mesons are reconstructed from γ pairs having an invariant mass within $\pm 15\,\mathrm{MeV}/c^2$ ($\pm 3\sigma$) of the π^0 nominal mass. Such combinations are then fitted with a π^0 mass constraint to improve the momentum resolution. ρ^+ mesons are reconstructed from $\pi^+\pi^0$ pairs having an invariant mass within $\pm 0.3\,\mathrm{GeV}/c^2$ of the nominal ρ^+ mass.

We reconstruct D^0 candidates using six decay modes [13]: $K^-\pi^+$, $K^-\pi^+\pi^0$, $K^-\pi^+\pi^+\pi^-$, $K^0_S\pi^+\pi^-$, K^-K^+ and $K^0_S\pi^0$, and D^+ candidates using decays to $K^0_S\pi^+$, $K^0_S\pi^+\pi^+\pi^-$, $K^-\pi^+\pi^+$ and $K^+K^-\pi^+$. A $\pm 15\,\mathrm{MeV}/c^2$ interval around the appropriate nominal D mass is used for all modes except for $D^0 \to K^-\pi^+\pi^0$, where we use a $\pm 25\,\mathrm{MeV}/c^2$ window, corresponding to about $\pm 3\sigma$ in each case. Selected D candidates are then subjected to a mass-vertex constrained fit to improve their momentum resolution. D^{*0} candidates are reconstructed via decays to $D^0\pi^0$ and $D^0\gamma$; the latter mode is not used for B_{sl} reconstruction because in this case the $D^*\pi$ invariant mass spectrum has a large background. D^{*+} candidates are reconstructed in two modes: $D^0\pi^+$ and $D^+\pi^0$. The mass difference $M(D^*)-M(D)$ for D^* candidates is required to be within $\pm 3\,\mathrm{MeV}/c^2$ (for $D\pi$) and $\pm 10\,\mathrm{MeV}/c^2$ (for $D^0\gamma$) intervals around the $m_{D^*} - m_D$ nominal value (about 3σ and 2σ, respectively). Reconstructed D^* candidates are subjected to a mass-vertex constrained fit.

For the signal B_{sl} meson side we form $D\ell$ (normalization mode) and $D^{(*)}\pi\ell$ (signal modes) combinations. The energy difference $\Delta E \equiv E_{\mathrm{tag}} - E_{\mathrm{CM}}$ and beam-constrained mass $M_{\mathrm{bc}} \equiv \sqrt{E^2_{\mathrm{CM}} - \vec{P}^2_{\mathrm{tag}}}$, (where E_{tag} and $\vec{P}_{\mathrm{tag}}$ are the tag B candidate center-of-mass (CM) energy and momentum and $E_{\mathrm{CM}} = \sqrt{s}/2 \simeq 5.29\,\mathrm{GeV}$) variables are used for B_{tag} selection. The B_{tag} signal region is defined as $M_{\mathrm{bc}} > 5.27\,\mathrm{GeV}/c^2$, $|\Delta E| < 40\,\mathrm{MeV}$, which is about 3σ in both cases. The B_{tag} candidates are subjected to an energy constrained fit to improve $\vec{P}_{\mathrm{tag}}$ resolution. We also use events from the $50\,\mathrm{MeV} < |\Delta E| < 130\,\mathrm{MeV}$ sidebands for background subtraction. In these events the B_{tag} candidate is fitted with its energy constrained to the center of the sideband. In the case of multiple entries in the signal region, the $B_{\mathrm{tag}}\,B_{\mathrm{sl}}$ candidate with the minimum χ^2_{tot} is chosen, where χ^2_{tot} is calculated as a sum over the χ^2 of intermediate D and D^* mesons mass (mass-vertex) fits and χ^2 of the B_{tag} energy fit. The same single candidate selection is applied to sidebands. The average number of candidates per event is 1.3 in each case.

The M^2_ν spectra for the four semileptonic decays $B \to D^{(*)}\pi\ell\nu$ are shown in Figs. 1, *1a)–1d)* as points with error bars. Clear peaks are evident in all distributions.

We divide the backgrounds into the following categories:

(1) Continuum $e^+e^- \to q\bar{q}$ events.

(2) Backgrounds with the B_{tag} misreconstructed from particles belonging to the other B meson or fake tracks.

(3) B_{sl} backgrounds with the B_{tag} reconstructed correctly, which can be further separated by their source:

(3a) Combinatorial background under the $D^{(*)}$ signal from $B_{\rm sl}$.

(3b) Hadrons misidentified as leptons.

(3c) Feed-down from $B \to D^*\pi\ell\nu$ reconstructed as $B \to D\pi\ell\nu$ with lost neutral(s).

All backgrounds except for (3c) are reliably determined and finally subtracted directly from the data. Backgrounds (1) and (2) are estimated using ΔE sidebands. Continuum data and generic $B\bar{B}$ MC simulation show that these backgrounds have flat ΔE distributions, thus justifying this procedure. Background (3a) is subtracted using $D^{(*)}$ ($M(D^{(*)})$) sidebands. However the region where backgrounds (2) and (3a) overlap is subtracted twice by using ΔE and $M(D^{(*)})$ sidebands. To account for this over-subtraction we use two-dimensional ΔE and $M(D^{(*)})$ sidebands. The sum of M_ν^2 distributions from one-dimensional $M(D^{(*)})$ and ΔE sidebands after subtraction of the two-dimensional sidebands are illustrated in Figs. 1, *1a)–1d)* by the hatched histograms. These histograms represent the sum of backgrounds (1), (2) and (3a).

Background (3b) is studied with data by using combinations of $D^{(*)}\pi$ with high momenta hadrons (h^+), where the h^+ candidate is selected with a lepton veto requirement. The combinatorial backgrounds are subtracted from the observed M_ν^2 distributions using ΔE and $M(D^{(*)})$ sidebands. The obtained M_ν^2 spectra are then multiplied by the known misidentification rate, which depends on the hadron laboratory momentum (see [14] for details). It is found that the remaining small peak around zero, which is due to the contribution of $B \to D^{(*)}\pi\pi^+(\pi^0)$ decays, is quite small ($\sim 0.5 - 1.0\%$) and we ignore it below, including it as a systematic error.

Background (3c) is observed only in the $B \to D\pi\ell\nu$ channels and is estimated from a MC simulation with normalization fixed to the data using $B \to D^*(\pi)\ell\nu$ signal yields. This contribution is plotted in Figs. 1, *1a), 1c)* as open histograms.

The background-subtracted M_ν^2 distributions are shown in Figs. 1, *2a)–2d)*. These distributions are fitted with signal functions, the shapes of which are fixed from MC studies. Fitted signal yields, reconstruction efficiencies and branching ratios are summarized in Table I. The branching ratios are calculated relative to the normalization modes $B \to D\ell\nu$ to cancel out the $B_{\rm tag}$ reconstruction efficiency according to the formula:

$$\mathcal{B}(mode) = \mathcal{B}(norm) \times \frac{N_{\rm mode}}{N_{\rm norm}} \times \frac{\epsilon_{\rm norm}}{\epsilon_{\rm mode}},$$

where $N_{\rm norm(mode)}$ and $\epsilon_{\rm norm(mode)}$ are the signal yield and reconstruction efficiency of the normalization mode (mode of interest) and the normalization mode $\mathcal{B}$ is taken from the PDG [15]. Relative efficiencies are obtained from MC simulation. Intermediate branching fractions are included, while the tagging efficiency is not. The reconstruction and background subtraction procedures for the $B \to D\ell\nu$ mode are identical to those applied for the studied channels. The obtained branching fractions are in good agreement with our previous measurement [8] and with BaBar results [9]. The low efficiency in the last mode is the result of not using the $D^{*0} \to D^0\gamma$ decay channel.

Signals for semileptonic B decays to orbitally excited D^{**} are extracted from the $D^{(*)}\pi$ invariant mass distributions. We define a signal window for $B \to D^{(*)}\pi\ell\nu$ decays by the requirement $|M_\nu^2| < 0.1\,{\rm GeV}^2/c^4$. The backgrounds are estimated in the same way as in the M_ν^2 distribution study. The $D^{(*)}\pi$ invariant mass spectra from the signal window after subtraction of backgrounds (1-3) are shown in Fig. 2. The mass distributions before background subtraction, restricted to the region near the $j_q = 3/2$ states, are shown in the insets.

TABLE I: Results for $B \to D^{(*)}\pi\ell\nu$ where the first error is statistical and the second is systematic.

Mode	Yield	Eff.,%	$\mathcal{B}$(mode),%
$B^+ \to \bar{D}^0\ell^+\nu$	2320 ± 60	6.4	2.15 ± 0.22 [a]
$B^+ \to D^-\pi^+\ell^+\nu$	192 ± 19	2.8	$0.40 \pm 0.04 \pm 0.06$
$B^+ \to D^{*-}\pi^+\ell^+\nu$	123 ± 14	1.14	$0.64 \pm 0.08 \pm 0.09$
$B^0 \to D^-\ell^+\nu$	760 ± 30	3.7	2.12 ± 0.20 [a]
$B^0 \to \bar{D}^0\pi^-\ell^+\nu$	150 ± 20	3.7	$0.42 \pm 0.07 \pm 0.06$
$B^0 \to \bar{D}^{*0}\pi^-\ell^+\nu$	22 ± 8	0.40	$0.56 \pm 0.21 \pm 0.08$

[a]Used as a reference.

To extract the D^{**} signals we perform simultaneous unbinned likelihood fits to the signal and background $D^{(*)}\pi$ mass spectra. The signal function includes all orbitally excited D^{**} contributing to the given final state (D_0 and D_2^* to $D\pi$ and D_1, D_1', D_2^* to $D^*\pi$), each of which is described by a relativistic Breit-Wigner function for a known orbital momenta, and a non-resonant part described by the Goity-Roberts model [16]. D^{**} masses and widths are fixed to measured values [6]. To further investigate the $D\pi$ mass spectrum we also test a $D_v^* + D_2^*$ hypothesis. Despite the $D^0\pi^+$ mass region corresponding to D^{*+} being excluded from the study, and while D^{*0} is below the $D^-\pi^+$ threshold, a virtual D_v^* can be produced off-shell. We describe the D_v^* contribution by a tail of the Breit-Wigner function with floating normalization. Fit results are shown as a dashed line for this combination.

A study of the sidebands shows that the background is described by the sum of a signal function and an exponential. The resulting signal function and contributions from the resonances are shown in Fig. 2 as solid and dashed curves, respectively, superimposed on the background-subtracted mass spectra. In the insets the solid and dashed curves represent the fitted signal and background, respectively. In $B^0 \to D^*\pi\ell\nu$ decays a small feature may be observed around $2.6\,\mathrm{GeV}/c^2$, which is absent in $B^+ \to D^*\pi\ell\nu$. However, the significance of this feature is small (2.5σ) and there is no known state there, so we do not include a term for it in the fit. Fitted resonance yields and corresponding product branching ratios are listed in Table II. The contribution of the non-resonant component in all cases is consistent with zero. The $B \to D^{**}\ell\nu$ decay significance is defined as $\sqrt{-2\ln L_{\max}/L_0}$, where L_0 is the likelihood value returned by the fit to the $D^{(*)}\pi$ distribution with the D^{**} contribution fixed to zero. Our result for $B \to \bar{D}_1\ell^+\nu$ is in good agreement with previous measurements [7]. For a $D_0^* + D_2^*$ hypothesis the branching ratio of the decay to the wide D_0^* is large, in contrast to theoretical predictions [4]. However, the present statistics do not definitely exclude an interpretation of broadly distributed $D\pi^+$ events as the D_v^* tail.

For $D^{*,**}$'s decaying into $D\pi$ we perform a study of the helicity angle distributions, which is the angle between π momentum and the direction opposite to $B_{\rm sl}$-momentum in the $D^{*,**}$ rest frame. To extract the D_v^*, D_0^* and the D_2^* helicity distributions we perform a combined fit of the $M(D\pi)$ spectra for $D\pi$ combinations from both B^+ and B^0 in bins of helicity angle. The fit procedure is identical to that used for the $\mathcal{B}(B \to D^{*,**}\ell\nu)$ calculation. The results corrected for the efficiency are plotted in Fig. 3. D_2^* distributions for D_v^* and D_0^* hypothesis coincide within errors, so that only that for the $D_0^* + D_2^*$ case is shown in Fig. 3 c. The D_0^* helicity distribution is consistent with the $J = 0$ hypothesis ($\chi^2/ndf = 6.0/4$, where ndf is the number of degrees of freedom). The D_2^* helicity distribution is fitted

TABLE II: Results of the $D^{(*)}\pi^+$ pair invariant mass study. $\mathcal{B}(\text{mode}) \equiv \mathcal{B}(B \to D^{**}\ell\nu) \times \mathcal{B}(D^{**} \to D^{(*)}\pi^+)$. The first error is statistical and the second is systematic.

Mode	Yield	$\mathcal{B}$(mode),%	Signif.
$B^+ \to \bar{D}_0^{*0}\ell^+\nu$	102 ± 19	$0.24 \pm 0.04 \pm 0.06$	5.4
$B^+ \to \bar{D}_2^{*0}\ell^+\nu$	94 ± 13	$0.22 \pm 0.03 \pm 0.04$	8.0
$B^0 \to D_0^{*-}\ell^+\nu$	61 ± 22	$0.20 \pm 0.07 \pm 0.05$	2.6
		< 0.4 @ 90% C.L.	
$B^0 \to D_2^{*-}\ell^+\nu$	68 ± 13	$0.22 \pm 0.04 \pm 0.04$	5.5
$B^+ \to \bar{D}_1^{'0}\ell^+\nu$	-5 ± 11	< 0.07 @ 90% C.L.	
$B^+ \to \bar{D}_1^{0}\ell^+\nu$	81 ± 13	$0.42 \pm 0.07 \pm 0.07$	6.7
$B^+ \to \bar{D}_2^{*0}\ell^+\nu$	35 ± 11	$0.18 \pm 0.06 \pm 0.03$	3.2
$B^0 \to D_1^{'-}\ell^+\nu$	4 ± 8	< 0.5 @ 90% C.L.	
$B^0 \to D_1^{-}\ell^+\nu$	20 ± 7	$0.54 \pm 0.19 \pm 0.09$	2.9
		< 0.9 @ 90% C.L.	
$B^0 \to D_2^{*-}\ell^+\nu$	1 ± 6	< 0.3 @ 90% C.L.	

with the function $a_0^2|Y_2^0|^2 + 4a_1^2|Y_2^1|^2 + 4a_2^2|Y_2^2|^2$, where the Y_j^i are spherical harmonics and $a_0^2 + 4a_1^2 + 4a_2^2 = 1$. The fit yields $a_0^2 = 0.74 \pm 0.10$, $a_1^2 = 0.04 \pm 0.02$ and $a_2^2 = 0.02 \pm 0.02$; the fit quality is $\chi^2/ndf = 2.0/3$. The fit is consistent with the assumed quantum numbers and demonstrates that the D_2^* from semileptonic decay is dominantly in the $s_z = 0$ spin projection. Helicity distributions, predicted by theory, are shown as dashed lines. For evaluating the $D_v^* + D_2^*$ hypothesis, the obtained D_v^* helicity distribution (Fig. 3 b) is fitted with the function $b_0^2|Y_1^0|^2 + b_1^2|Y_1^1|^2$. This fit yields $b_0^2 = 0.15 \pm 0.09$, $b_1^2 = 0.85 \pm 0.09$ ($\chi^2/ndf = 18.8/4$) in poor agreement with expectations from theory, shown as a dashed line.

We also study the dependence of the $B \to D^{**}$ transition on q^2 or, equivalently, on the conventional HQET variable w, which is the dot-product of B and D^{**} four-velocities: $w = v_B \cdot v_{D^{**}}$. The w-dependence is obtained from fits of $D\pi$ invariant mass in bins of w. The results are presented in Fig. 4. As with the helicity study the D_2^* distribution is shown only for the $D_0^* + D_2^*$ hypothesis in Fig. 4 c. The w distribution is fitted according to the model given in Ref. [17]. In HQET, the matrix elements between the B and D states to leading order in $\Lambda_{\rm QCD}/m_Q$ are expressed in terms of three universal Isgur-Wise functions $\xi(w)$, $\tau_{1/2}(w)$ and $\tau_{3/2}(w)$ for (D, D^*), (D_0^*, D_1') and (D_1, D_2^*) doublets, respectively [17]. We assume a "pole" form for $\xi(w)$: $\xi = (2/(1+w))^{2\rho^2}$ and a linear form for $\tau_i(w)$ functions: $\tau_i(w) = \tau_i(1)[1 + \hat{\tau}_i'(w-1)]$, and the following relation: $\hat{\tau}_{1/2}' = \hat{\tau}_{3/2}' + 0.5$ [18]. A simultaneous fit to the w-distributions for D_0^* and D_2^* gives $\hat{\tau}_{3/2}' = -1.8 \pm 0.3$. Using the measured branching ratios of $B \to D_{0,2}^*\ell\nu$, we also calculate $\tau_{3/2}(1) = 0.75$ and $\tau_{1/2}(1) = 1.28$. All parameters are in agreement with expectations except for $\tau_{1/2}(1)$, which is larger than predicted due to the large value of $\mathcal{B}(B \to D_0^*\ell\nu)$.

The systematic error in the calculation of branching fractions due to $B_{\rm tag}$ efficiency uncertainty cancelled out since normalization modes were used. The largest contribution to the systematic error is from uncertainty in D^{**} parameters. We perform a $D^{(*)}\pi$ mass study with these parameters allowed to float inside their errors to get it. The $B_{\rm sl}$ reconstruction

efficiency dependence due to the decay model was studied using two different signal MC samples generated with the ISGW2 [19] and Goity-Roberts [16] models. To estimate the systematic uncertainty in background subtraction we used two different sets of sidebands with appropriate normalizations. To estimate interference effects we perform MC study with different angle efficiency dependencies. A summary of the systematic error contributions is presented in Table III. In total we obtain a 14% error for the $B \to D^{(*)}\pi\ell\nu$ measurement, a 16% error for the narrow D^{**} contribution and 25% for the measurement of the wide D^{**} contribution.

TABLE III: Sources of systematic error.

Source of error	Systematic error, %
Reconstruction	2
Model efficiency	7
Background subtraction	6
Misidentified hadrons	1
Interference	7
Normalization branching ratios	10
D^{**} parameters	6–20
Total	14–25

In conclusion, we report measurements of the branching fractions for $B \to D^{(*)}\pi\ell\nu$ decays. These measurements supersede our previous results [8]. We also performed an analysis of the final state $D^{(*)}\pi$ hadronic system and obtained branching ratios for the $B \to D^{**}\ell\nu$ components. Semileptonic decay to D_2^* meson is observed and measured for the first time. Helicity and w distributions are studied for this decay. We observe a broad enhancement in the $D\pi$ mass distribution consistent with wide D_0^* production. The branching ratio of the decay to $B \to D_0^*\ell\nu$ is found to be large, in contrast with theoretical predictions [4]. However there is no indication of a broad D_1' in the $B \to D^*\pi\ell\nu$ channel, which should be of the same order. The combined likelihood of fits to the $D\pi$ mass, helicity and w distributions for $D_0^* + D_2^*$ hypothesis is higher than that for the $D_v^* + D_2^*$ combination by 2.8σ.

However, the present data sample cannot exclude the interpretation of this enhancement as a D_v^* tail.

We would like to thank I.I. Bigi for useful discussions.

We thank the KEKB group for the excellent operation of the accelerator, the KEK cryogenics group for the efficient operation of the solenoid, and the KEK computer group and the National Institute of Informatics for valuable computing and Super-SINET network support. We acknowledge support from the Ministry of Education, Culture, Sports, Science, and Technology of Japan and the Japan Society for the Promotion of Science; the Australian Research Council and the Australian Department of Education, Science and Training; the National Natural Science Foundation of China under contract No. 10575109 and 10775142; the Department of Science and Technology of India; the BK21 program of the Ministry of Education of Korea, the CHEP SRC program and Basic Research program (grant No. R01-2005-000-10089-0) of the Korea Science and Engineering Foundation, and the Pure Basic

Research Group program of the Korea Research Foundation; the Polish State Committee for Scientific Research; the Ministry of Education and Science of the Russian Federation and the Russian Federal Agency for Atomic Energy; the Slovenian Research Agency; the Swiss National Science Foundation; the National Science Council and the Ministry of Education of Taiwan; and the U.S. Department of Energy.

[1] O.L. Buchmuller, H.U. Flacher, Phys. Rev. D**73**, 073008 (2006); K. Abe *et al.* (Belle Collaboration), BELLE-CONF-0669, hep-ex/0611047; B. Aubert *et al.* (BaBar Collaboration), arXiv:0707.2670.
[2] N. Uraltsev, Phys. Lett. B**501**, 86 (2001).
[3] N. Uraltsev, hep-ph/0409125.
[4] I.I. Bigi *et al.*, Eur. Phys. J. C**52**, 975 (2007).
[5] J. Rosner, Comm. Nucl. Part. Phys. **16**, 109 (1986).
[6] K. Abe *et al.* (Belle Collaboration), Phys. Rev. D **69**, 112002 (2004); A. Kuzmin *et al.* (Belle Collaboration), Phys. Rev. D **76**, 012006 (2007).
[7] D. Buskulic *et al.* (ALEPH Collaboration), Z. Phys. C **73**, 601 (1997); A. Anastassov *et al.* (CLEO Collaboration), Phys. Rev. Lett. **80**, 4127 (1998); V.M. Abazov *et al.* (D0 Collaboration), Phys. Rev. Lett. **95**, 171803 (2005); J. Abdallah *et al.* (DELPHI Collaboration), Eur. Phys. J. C **45**, 35 (2006).
[8] D. Liventsev *et al.* (Belle Collaboration), Phys. Rev. D **72**, 051109 (2005).
[9] B. Aubert *et al.* (BaBar Collaboration), arXiv:0708.1738.
[10] S. Kurokawa and E. Kikutani, Nucl. Instr. and. Meth. A **499**, 1 (2003), and other papers included in this volume.
[11] A. Abashian *et al.* (Belle Collaboration), Nucl. Instr. and Meth. A **479**, 117 (2002).
[12] Z. Natkaniec *et al.* (Belle SVD2 Group), Nucl. Instr. and Meth. A **560**, 1 (2006).
[13] Throughout this paper, the inclusion of the charge-conjugate decay modes is implied unless otherwise stated.
[14] C. Schwanda *et al.* (The Belle Collaboration), Phys. Rev. D **75**, 032005 (2007).
[15] W.-M. Yao *et al.* (Particle Data Group), J. Phys. G **33**, 1 (2006).
[16] J.L. Goity, W. Roberts, Phys. Rev. D **51**, 3459 (1995).
[17] A. Le Yaouanc *et al.*, Phys. Lett. B **520**, 25 (2001).
[18] S. Veseli, M.G. Olsson, Phys. Lett. B **367**, 302 (1996).
[19] D. Scora and N. Isgur, Phys. Rev. D **52**, 2783 (1995); N. Isgur, D. Scora, B. Grinstein, M. B. Wise, Phys. Rev. D **39**, 799 (1989).

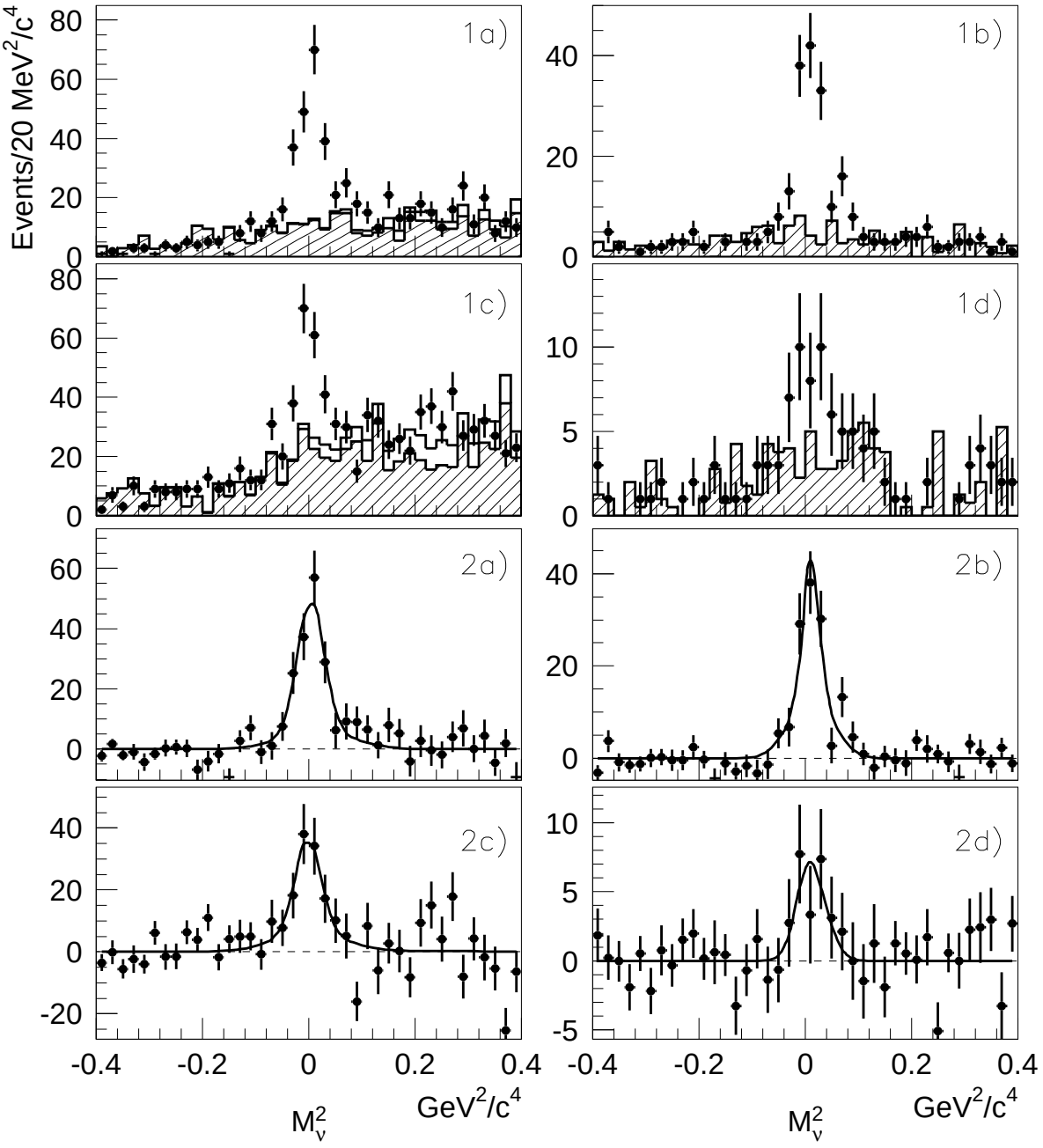

FIG. 1: M_ν^2 spectra before (1) and after (2) background subtraction for: *a)* $B^+ \to D^-\pi^+\ell^+\nu$, *b)* $B^+ \to D^{*-}\pi^+\ell^+\nu$, *c)* $B^0 \to \bar{D}^0\pi^-\ell^+\nu$, *d)* $B^0 \to \bar{D}^{*0}\pi^-\ell^+\nu$. The curves are the fits, which are described in the text.

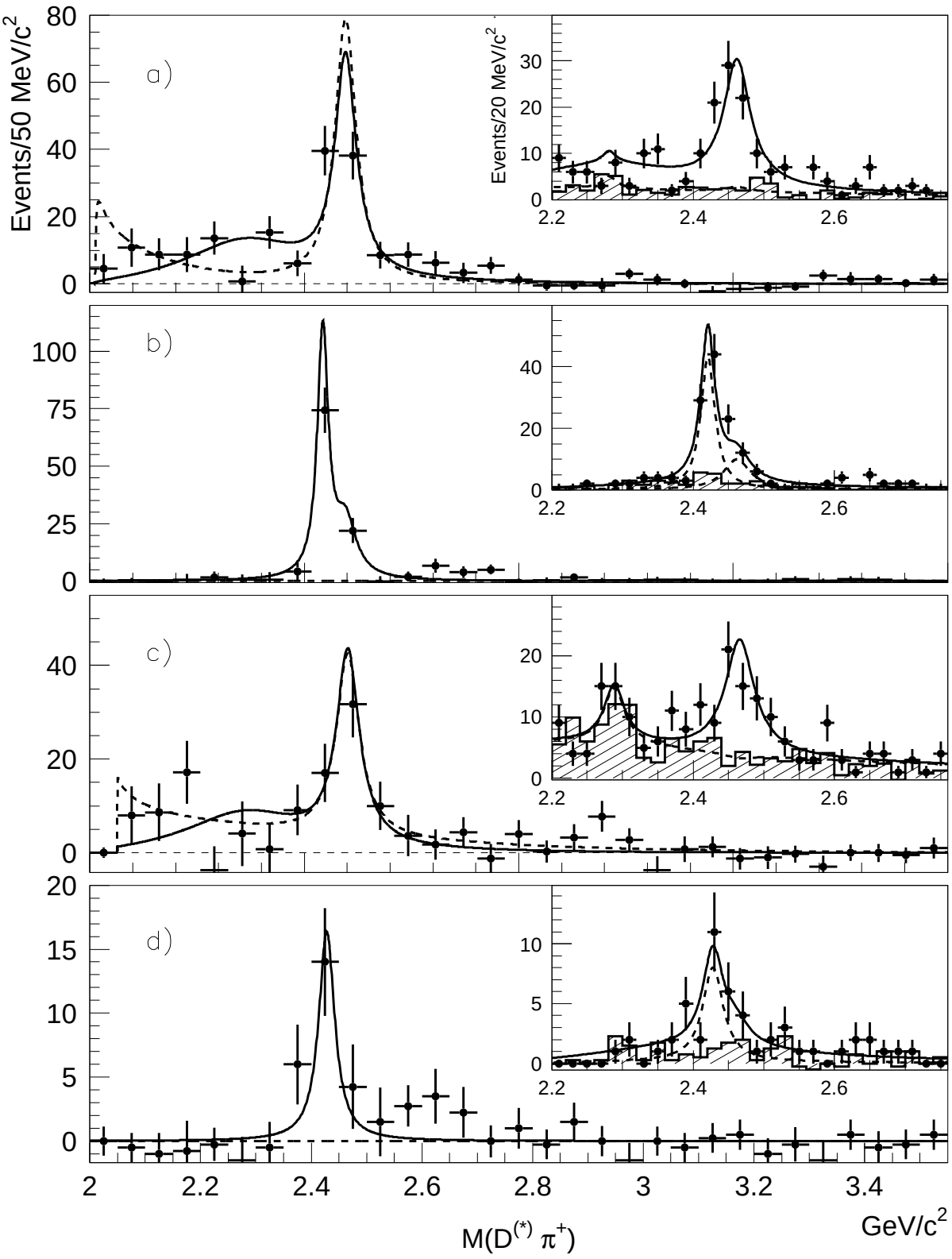

FIG. 2: Hadronic invariant mass distributions for: *a)* $B^+ \to D^-\pi^+\ell^+\nu$, *b)* $B^+ \to D^{*-}\pi^+\ell^+\nu$, *c)* $B^0 \to \bar{D}^0\pi^-\ell^+\nu$, *d)* $B^0 \to \bar{D}^{*0}\pi^-\ell^+\nu$. Insets show the distributions before background subtraction in the region around the narrow D^{**}'s. The background is shown as the hatched histogram. The curves are the fits, which are described in the text.

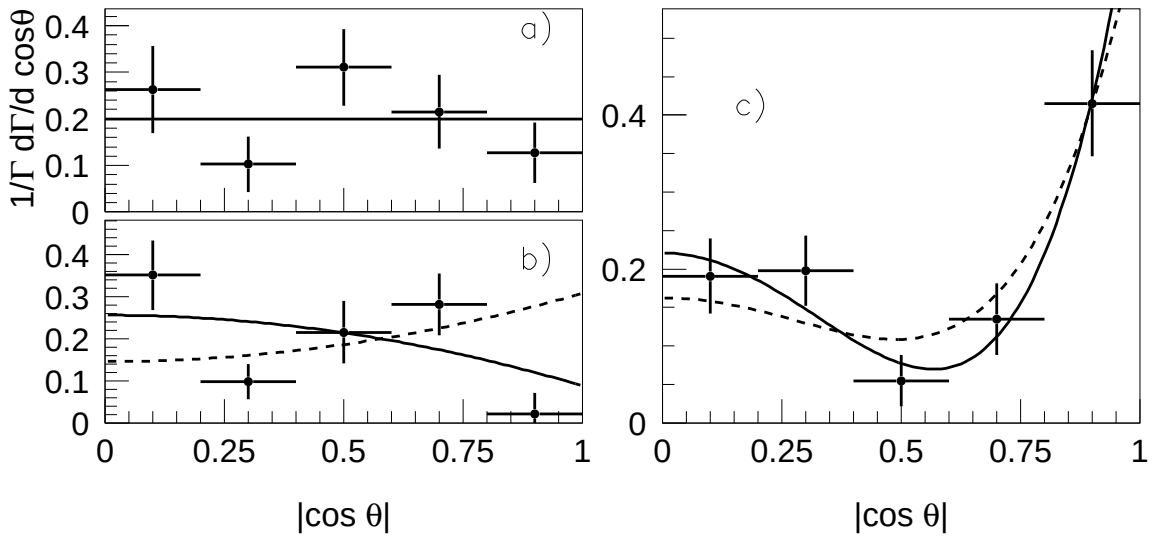

FIG. 3: Helicity distributions for *a)* D_0^*, *b)* D_v^*, *c)* D_2^*. The curves represent the fits, described in the text.

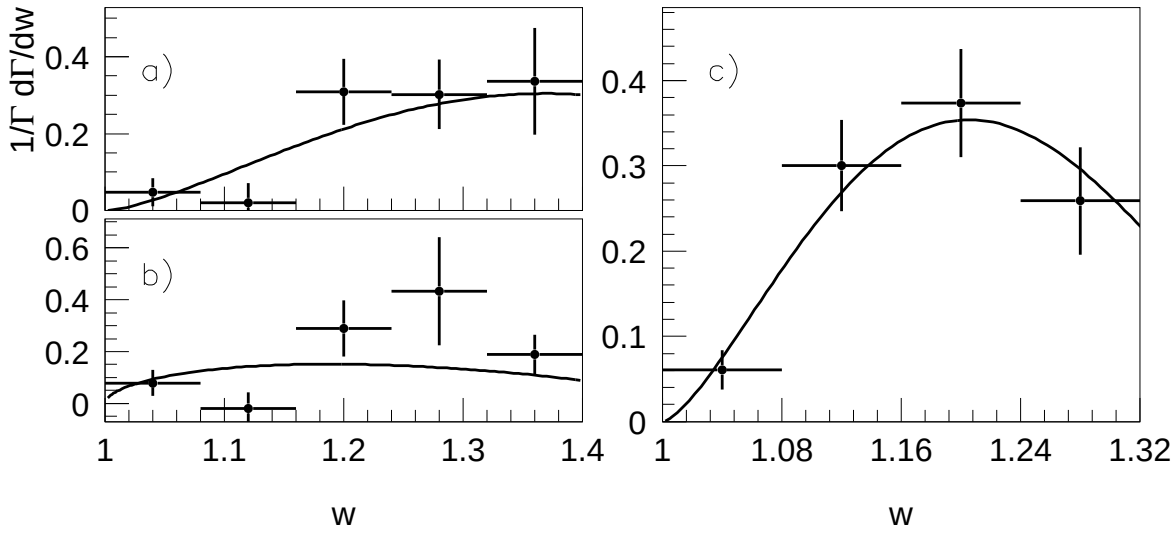

FIG. 4: w distributions for *a)* D_0^*, *b)* D_v^*, *c)* D_2^*. The curves are the fits, which are described in the text.